Optical Interference Effects in Visible-Near Infrared Spectral Range for Arrays of Vertically Aligned Multiwalled Carbon Nanotubes

M. Wąsik*, J. Judek, K. Świtkowski and M. Zdrojek
Faculty of Physics, Warsaw University of Technology, Koszykowa 75, 00-662 Warsaw, Poland

(Received February 5, 2016; in final form December 30, 2016)

Based on the reflectance spectra for radiation wavelength from about 380 nm to 1.8 μm, the optical interference effects in vertically aligned multiwalled carbon nanotubes films are studied. We performed the measurements for two complementary polarization states of incoming radiation (s- and p-polarization) for nanotubes arrays sparse enough for interference effects to be possible to observe. By performing the measurements for different wavelengths and incidence angles, we mapped the evolution of interference maxima/minima of reflectance signal. The results from this novel approach indicate that for the radiation polarized perpendicularly to tubes axis (s-polarization), the real part of the effective refractive index can be estimated from the classic Fabry–Pérot model. In order to describe the differences between spectra obtained for s- and p-polarizations we discuss the most important factors that affect the reflectance signal in case of investigated nanotubes arrays.

DOI: 10.12693/APhysPolA.131.232
PACS/topics: 78.20.Ci, 78.67.Ch, 81.07.De

1. Introduction

As far as the optical properties of carbon nanotubes (CNTs) are concerned, one of the most prominent results of recent studies in this field is a possibility of manufacturing arrays of carbon nanotubes resembling the classic black bodies [1–3]. The typical investigated systems are ordered or random arrays of vertically aligned single- or multiwalled carbon nanotubes (MWCNTs), usually produced by chemical vapor deposition method [4]. The high value of aspect ratio of a singlewalled carbon nanotube allows only for a preparation of arrays of mutually supported tubes, whereas MWCNTs offer a high flexibility in designing the structural parameters of an array. The most important ones include single tube's diameter and length, density of packaging (also called as fill factor), and (optionally) required pattern.

The blackbody behavior of carbon nanotubes arrays manifesting itself with extremely low reflectance level [2, 5] is related to a process of trapping and multiple reflections of electromagnetic radiation within a sparse array of MWCNTs [6, 7]. For a quantitative discussion of this issue and other optical phenomena in such systems, two approaches are usually applied. A starting point for both cases is an assumption that a single CNT can be modelled as a homogeneous hollow cylinder described by an inner and an outer radius and with the optical properties derived from bulk graphite [8]. If the investigated CNTs array is periodic in space (which is achieved by periodic patterning of catalyst particles before the growth process) then the full information about the radiation propagating in the system can be obtained by numerical solving of the Maxwell equations with the use of finite difference time domain method [9–11].

The second approach consists in treating the CNT array as an effective homogeneous material whose optical properties are determined by properties of both host material (e.g. air or polymer) and inclusions (CNTs) [12, 13]. The advantage of this model is the fact that it allows for formulating the explicit expressions (at least in principle) describing the experimentally measurable quantities like absorption or reflectance [14, 15]. In this article we apply this approach for explaining the evolution of the observed reflectance signal from the arrays of random, vertically aligned MWCNTs. The assumption about homogeneity of the optical layer formed by CNTs allows us for the use of classical Fabry–Pérot theory that predicts the observation of interference effects in the measured optical signals. The way we present for obtaining the quantitative and qualitative description of optical properties of MWCNT arrays has not been so far demonstrated in the literature. Particularly, the analysis of reflectance maps included in the article is a new idea in the discussed field.

2. Materials and methods

We used the commercially available (NanoLab Inc.) samples of vertically aligned carbon nanotubes arrays grown by chemical vapor deposition on silicon substrates covered with a layer of chromium. To study the interference effects we chose two samples (labeled A and B) of free-standing MWCNTs with random distributions of tubes in both cases (Fig. 1). The averaged diameter/length of the tubes are equal to 75 nm/1.5 μm (sample A) and 40 nm/1 μm (sample B) and the site density (number of tubes per unit area) was the same for both samples and

*corresponding author; e-mail: wasik@if.pw.edu.pl

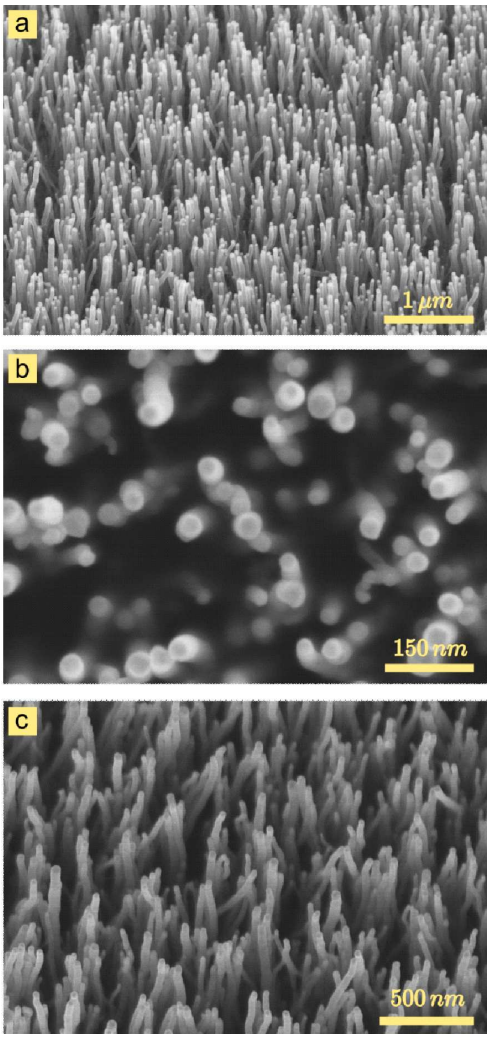

Fig. 1. Scanning electron microscope images of the investigated samples: sample A (general view (a)), sample B (top view (b), general view (c)).

approximately equal to 10^9 cm^{-2}. These numbers correspond to fill factors of about 4.4% (A) and 1.3% (B). Apart from the described samples we also used MWCNT arrays of much larger heights and site densities, but as we expected, the absorption level made it impossible to observe the interference effects. For these reason, for a further analysis, two representative samples presented above were chosen.

The structural parameters of the investigated samples make them systems exhibiting low reflectance which dictates the use of either a high power radiation source or a sensitive detection scheme for experiments. In the presented research we used the optical setup with a halogen lamp, a monochromator (Newport/Oriel Instruments) and polarization optics. Additionally, for improving the signal-to-noise ratio we adopted the setup to the lock-in detection (Fig.Â˘2). Signal was modulated by placing an optical chopper in a path of a light beam. The sam-

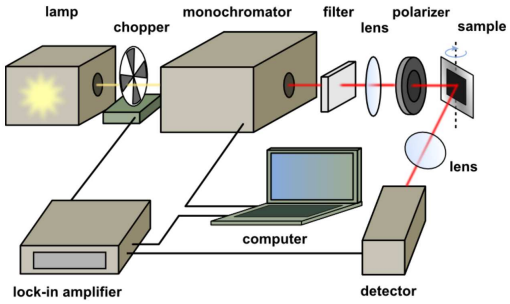

Fig. 2. General scheme of experimental setup used in the experiment. A sample is placed in a rotational holder and the position of a detector is adjusted to the changing path of reflected radiation.

ples of MWCNT arrays were placed in a rotational holder which allowed for incidence angle control. The width of a light beam on the sample under normal incidence was about 2 mm. For radiation intensity measurements we used silicon and germanium detectors. Two fundamental polarization states of incoming radiation were provided: *s*- and *p*-type polarization direction perpendicular and parallel to the plane of incidence, respectively.

3. Results and discussion

The measurements of the reflected radiation intensity were performed in the spectral range from 380 nm to 1.8 μm and for incidence angle (θ) from 10° to 80°. The given values of the extreme incidence angles are a consequence of the geometrical limitations of the optical setup and the size of the radiation spot for higher θ. Figure 3 shows some exemplary reflectance spectra (ratio of reflected and incoming light intensities) obtained for sample A, where characteristic oscillatory pattern can be recognized [16–18]. Such behavior of reflectance signal is ascribed to a specific form of interference phenomenon commonly known as Fabry–Pérot or etalon effect. If the radiation reflected from the top surface of the nanotubes forest interferes with radiation penetrating the array and being reflected from the substrate, then the general reflectance spectrum is modified with the interference maxima and minima.

The obtained spectra combined into the maps of reflectance as a function of wavelength and incidence angle $R(\lambda, \theta)$ are presented in Fig. 4. The measuring steps for λ and θ were equal to 1 nm and 5°, respectively. To emphasize the details of the reflectance signal, all the maps present the logarithm of $R(\lambda, \theta)$ and the grid of discrete R values were smoothed (without loss to the physical interpretation). The reflectance maps for both *s*- and *p*-polarization reveal the presence of series of maxima and minima whose positions on wavelength axis depend on the incidence angle.

Theoretical considerations for an arbitrary isotropic thin film characterized by a complex dielectric function lead to the explicit formula describing the reflectance

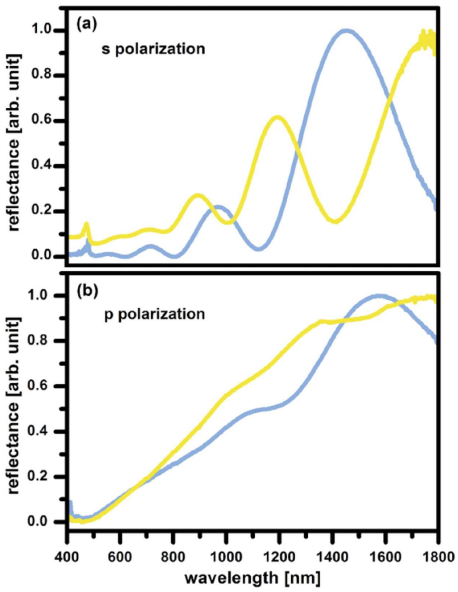

Fig. 3. Normalized reflectance spectra for s- (a) and p-polarization (b). The blue and yellow curves correspond to sample A and B, respectively. Incidence angle $\theta = 60^\circ$ for all spectra.

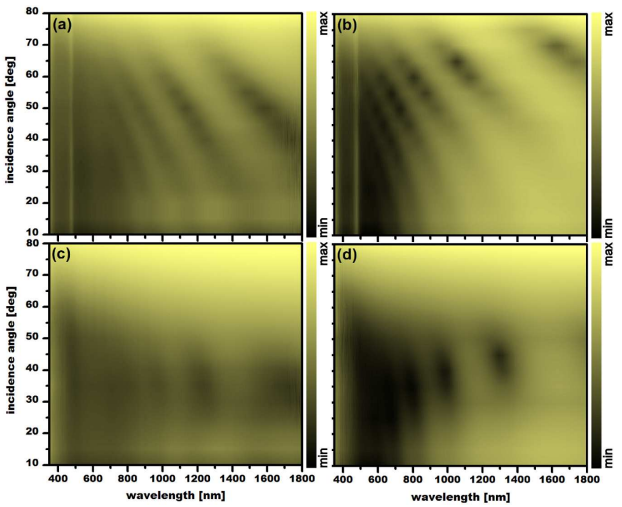

Fig. 4. Reflectance maps $R(\lambda, \phi)$ for s-polarization — sample A/B (b)/(a) and p-polarization — sample A/B (d)/(c). The color scale represents the logarithm of reflectance signal.

spectrum of the given sample. The expression for polarization-dependent reflectance $R^{(s,p)}(\lambda, \theta)$ (Eq. (1)) contains the reflection coefficients $r_{ij}^{(s,p)}$ (complex numbers in general, a full form given e.g. in [19]) which are related through generalized Fresnel equations to optical constants of an investigated material and a substrate (interface materials labeled by i and j):

$$R^{(s,p)}(\lambda, \theta) = \left| \frac{r_{12}^{(s,p)} + r_{23}^{(s,p)} \exp(\mathrm{i}\phi - \alpha d)}{1 + r_{12}^{(s,p)} r_{23}^{(s,p)} \exp(\mathrm{i}\phi - \alpha d)} \right|^2 . \qquad (1)$$

The complexity of Eq. (1) lies in fact that $r_{ij}^{(s,p)}$, ϕ (phase difference between consecutive interfering rays), α (absorption coefficient) and d (effective path length of light) are all functions of wavelength, incidence angle or both of them. In consequence, the final form of the reflectance signal is a combination of optical properties of the material constituting the thin layer and geometrical factors which are essential for observation of interference oscillations [20].

Based on the above discussion it becomes clear that the precise positions of the local maxima/minima of $R^{(s,p)}(\lambda, \theta)$ are determined by all constants appearing in Eq. (1). Since we are unable to find the analytical expression for those extremes we have to simplify the general model and compare its predictions with the experimental results. As far as the effective refractive index of MWCNT arrays is concerned ($\varepsilon_{\mathrm{eff}} = n_{\mathrm{eff}} + \mathrm{i}\kappa_{\mathrm{eff}}$), it is known that such systems owe its extremely low reflectance to a specific values of n_{eff} and κ_{eff} [1]. If the condition $\kappa/n \ll 1$ is satisfied, then the radiation propagates approximately according to the simple geometrical optics laws [19] and phase difference ϕ appearing in Eq. (1) can be easily established. The validity of the above condition for low density CNT arrays can be supported by analyzing the values of κ/n calculated theoretically in the literature: ≈ 0.036 — visible range [7] and ≈ 0.0096 — visible range [1]. Assuming that coefficients $r_{ij}^{(s,p)}$ smoothly depend on wavelength and incidence angle, we can show that the extremes of the function $R^{(s,p)}(\lambda, \theta)$ are mainly determined by the extremes of the function $\phi(\lambda, \theta)$. After the appropriate calculations, the values of wavelengths for which the extremes $\lambda_{\mathrm{ext}}^{(m)}(\theta)$ occur, are found in the form given by Eq. (2):

$$\lambda_{\mathrm{ext}}^{(m)}(\theta) = \frac{4L}{m} \sqrt{n_{\mathrm{eff}}^2 - n_1^2 \sin^2 \theta}, \qquad (2)$$

where L is a thickness of a considered layer (known from the scanning electron microscopy (SEM) measurements), m is an integer index numbering the extremes and n_1 is a real part of the refractive index of a medium whose radiation is coming from (for air $n_1 = 1$). The information about κ_{eff} is lost in Eq. (2) but we have the straightforward expression relating $\lambda_{\mathrm{ext}}^{(m)}(\theta)$ and n_{eff}. Also, the lack of substrate properties influence in Eq. (2) is equivalent to considering it as a kind of a mirror (at least in the discussed spectral range) having no specific features in its reflection spectrum. For the s-polarization, the experimental results presented in the maps from Fig. 4 confirm that the interference extremes do follow the pattern determined by Eq. (2). The exemplary curves demonstrating the agreement with the proposed simplified model are shown in Fig. 5. From the fitting procedure we obtained the values of n_{eff} describing both samples of the MWCNT arrays for s-polarization. The averaged values of n_{eff} calculated based on curves for different m are equal to 1.17 (sample A) and 1.08 (sample B). The obtained

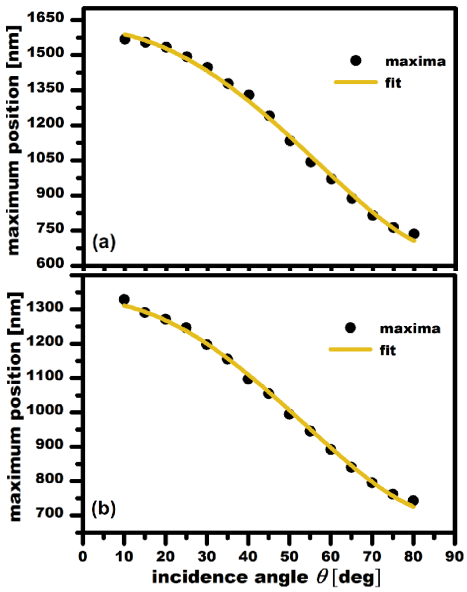

Fig. 5. Angular evolution of spectral positions of the selected interference maxima for s polarization, sample A (a) and B (b), $n_1 = 1$. The theoretical curves fitted according to Eq. (2).

values cannot be directly compared to the ones presented in the literature since effective optical constants strongly depend on structural parameters of arrays and they considerably differ between the reports. However, it is seen that the higher value of n_{eff} corresponds to the sample with higher density (sample A) which is the reasonable result in view of the effective medium theory. The detailed experimental analysis of how individual structural parameters of MWCNT arrays influence optical spectra and n_{eff} would require a large number of samples differing in e.g. site densities or tube diameter. Such studies could be an interesting continuation of the presented research.

From the comparison of the maps from Fig. 4, it is clearly seen that the behaviour of interference extremes for p-polarization is qualitatively different. In this case the extremes are less pronounced and, more importantly, their evolution is poorly described by Eq. (2), both in case of sample A and sample B. Such situation where the experimental results for reflectance spectra agrees with analytical model only for s-type polarization has been reported in literature [18] and its origin is found in the complexity of Eq. (1). Two possible factors may play a special role in explaining this issue. Firstly, the angular dependence of reflectance $R(\theta)$ of a typical metal substrate for s-polarization is an increasing function of θ, whereas p-polarization corresponds to $R(\theta)$ with local minimum. Secondly, if the condition $n_1 < n_2$ is satisfied (which is valid in our experiment) then the reflection coefficients $r_{12}^{(s)}$ are positive numbers irrespective of the θ value. The same statement in case of $r_{12}^{(p)}$ coefficients is not valid and consequently the simplifications made to $R^{(p)}(\lambda, \theta)$ function become less justified.

It should be noted that the procedures allowing for determination of effective refractive index for carbon nanotubes arrays have been already presented in some works [1, 18] however the authors do not usually consider the details of the proposed models. To our best knowledge our work is the first one which demonstrates the simple method for estimation of n_{eff} with the use of $R(\lambda, \theta)$ reflectance maps.

4. Conclusions

To sum up, we conducted the study of the reflectance signal coming from vertical arrays of MWCNT paying special attention to the observed interference patterns. By performing the measurements for different incidence angles and for spectral range from visible to near infrared it was possible to demonstrate the evolution of interference extremes originating from the Fabry–Pérot effect. Based on the obtained results we proposed the simple model relating the positions of interference extremes to a real part of the effective refractive index of MWCNT arrays. It turns out that the agreement between the model and experimental results is satisfactory only if the incoming radiation is s-polarized which is the restriction observed also in the previous reports in this field.

Acknowledgments

This research was funded by Polish Ministry of Science and Higher Education under Diamond Grant [No. DI 2011029441].

References

[1] H. Shi, J.G. Ok, H. Won Baac, L. Jay Guo, *Appl. Phys. Lett.* **99**, 211103 (2011).

[2] T. Saleh, M.V. Moghaddam, M.S. Mohamed Ali, M. Dahmardeh, C.A. Foell, A. Nojeh, K. Takahata, *Appl. Phys. Lett.* **101**, 061913 (2012).

[3] K. Mizuno, J. Ishii, H. Kishida, Y. Hayamizu, S. Yasuda, D.N. Futaba, M. Yumura, K. Hata, *Proc. Natl. Acad. Sci. USA* **106**, 6044 (2009).

[4] Z. Ren, Y. Lan, Y. Wang, *Aligned Carbon Nanotubes*, Springer, Heidelberg 2013.

[5] Z.P. Yang, L. Ci, J.A. Bur, S.Y. Lin, P.M. Ajayan, *Nano Lett.* **8**, 446 (2008).

[6] M. Wąsik, J. Judek, M. Zdrojek, A.M. Witowski, *Mater. Lett.* **137**, 85 (2014).

[7] K.C. Hsieh, T.Y. Tsai, D. Wan, H.L. Chen, N.H. Tai, *ACS Nano* **4**, 1327 (2010).

[8] A.B. Djurišić, E.H. Li, *J. Appl. Phys.* **85**, 7404 (1999).

[9] H. Bao, X. Ruan, T.S. Fisher, *Opt. Express* **18**, 6347 (2010).

[10] Y. Shamsollahi, M.K. Moravvej-Farshi, M. Ebnali-Heidari, *J. Lightwave Technol.* **31**, 1946 (2013).

[11] X.H. Wu, L.S. Pan, X.J. Fan, D. Xu, H. Li, C.X. Zhang, *Nanotechnology* **14**, 1180 (2003).

[12] W. Lü, J. Dong, Z.Y. Li, *Phys. Rev. B* **63**, 033401 (2000).

[13] F.J. García-Vidal, J.M. Pitarke, J.B. Pendry, *Phys. Rev. Lett.* **78**, 4289 (1997).

[14] X.J. Wang, L.P. Wang, O.S. Adewuyi, B.A. Cola, Z.M. Zhang, *Appl. Phys. Lett.* **97**, 163116 (2010).

[15] H. Ye, X.J. Wang, W. Lin, C.P. Wong, Z.M. Zhang, *Appl. Phys. Lett.* **101**, 141909 (2012).

[16] D.H. Kim, H.S. Jang, C.D. Kim, D.S. Cho, H.S. Yang, H.D. Kang, B.K. Min, H.R. Lee, *Nano Lett.* **3**, 863 (2003).

[17] H. Bao, B. Duvvuri, M. Lou, X. Ruan, *J. Quant. Spectrosc. Radiat. Transfer* **132**, 22 (2013).

[18] T. De Los Arcos, P. Oelhafen, D. Mathys, *Nanotechnology* **18**, 265706 (2007).

[19] P.C.Y. Chang, J.G. Walker, K.I. Hopcraft, *J. Quant. Spectrosc. Radiat. Transfer* **96**, 327 (2005).

[20] M.A. Kats, R. Blanchard, P. Genevet, F. Capasso, *Nat. Mater.* **12**, 20 (2013).